Bioinspiration &
Biomimetics

PAPER • **OPEN ACCESS**

A minimalistic walking fish robot twin based on the single actuator wave-like mechanism

To cite this article: Narges Khadem Hosseini *et al* 2026 *Bioinspir. Biomim.* **21** 016002

Bioinspiration & Biomimetics

PAPER

A minimalistic walking fish robot twin based on the single actuator wave-like mechanism

Narges Khadem Hosseini[1,*], Michael Ishida[1], Fidji Berio[2], Valentina Di Santo[2] and Fumiya Iida[1]

[1] Department of Engineering, University of Cambridge, Trumpington St, CB2 1PZ Cambridge, United Kingdom
[2] Scripps Institution of Oceanography, University of California, San Diego, 6500 Gilman Drive, La Jolla, CA 92093, United States of America
[*] Author to whom any correspondence should be addressed.

E-mail: nk616@cam.ac.uk, myi20@cam.ac.uk and fi224@cam.ac.uk

OPEN ACCESS

RECEIVED
3 May 2025

REVISED
3 November 2025

ACCEPTED FOR PUBLICATION
14 November 2025

PUBLISHED
11 December 2025

Keywords: bio-inspired robotics, terrestrial locomotion, *Polypterus senegalus*, robotic fish, single-actuator mechanism, wave-like motion, walking fish

Supplementary material for this article is available online

Abstract

Understanding terrestrial locomotion in walking fish species can unlock new insights into vertebrate evolution and inspire versatile robotic systems capable of traversing diverse environments. We introduce a novel, single-actuator continuum robot inspired by the terrestrial locomotion of the gray bichir (*Polypterus senegalus*), which employs a simple rotating helix to reproduce realistic undulatory movements. We hypothesized that a simplified robotic model with minimal actuation could accurately replicate the terrestrial locomotion patterns observed in *P. senegalus*. Using a 'robot-twin' methodology, we developed four helix configurations directly informed by the observed gait postures of real fish specimens and compared robotic performance and kinematics against biological data. We found that helix geometry significantly influenced both locomotion speed and lateral stability, with designs closely mimicking biological curvatures often exhibiting trade-offs between accuracy and performance. The fastest helix configuration produced the greatest lateral oscillation, whereas the most biologically accurate shape resulted in reduced locomotion efficiency. Additionally, integrating passive leg structures greatly enhanced stability, mirroring the biomechanical function of pectoral fins in the real fish. These findings underscore the value of minimalistic robotic designs in understanding fish-like locomotion and pave the way for future robotic platforms using reduced degrees of freedom.

1. Introduction

One of the fundamental intersections between biology and mechanics is the study of locomotion. For biological organisms and engineered systems alike, the type of locomotion that an agent employs is heavily dependent on the environment in which it moves. Animals capable of multi-modal locomotion are often highly adapted for movement in one medium but can deploy alternative, less efficient gaits in others. For instance, while the streamlined morphology of fishes is optimized for swimming, some species are also capable of walking on land [1]. Although fish swimming mechanics are well characterized, their terrestrial walking remains comparatively understudied, leaving many open questions about how organisms adapted for aquatic life overcome the challenges of moving on land.

A common technique for studying locomotion is the use of bioinspired robots to collect structured data systematically with well-defined input and output signals. Researchers can design robots with the exact desired morphologies and generate known motions for controlled experiments that follow the *ceteris paribus* principle (i.e. one feature of interest is varied while all other features remain constant) [2]. Furthermore, since locomotion is governed by the forces and interactions between the system and the environment, physical robots are valuable for studying locomotion as they can provide insights into processes that depend on the interactions between the system and the real world [3, 4]. Physical experiments with bioinspired robots not only can reproduce

biological phenomena but can also generate new hypotheses about living organisms, which can then be tested through biological experiments [5]. This reciprocal approach, often termed the 'robot-twin' paradigm, highlights the two-way exchange between biology and engineering: biological systems inspire better robotic designs, while robotic models uncover new insights into the natural world.

To model the locomotion of walking fish with a bioinspired robot, we took inspiration from the gray bichir *Polypterus senegalus*, which walks by planting a pectoral fin against the ground and articulating its spinal column to pivot its body around the stationary fin [6]. *P. senegalus* displays intraspecific differences between its walking kinematics and swimming kinematics [7], indicating the importance of a model specific to the walking motion of *P. senegalus*. Furthermore, there are considerable interspecific differences in morphology and motion between fish to consider when adapting other existing models of locomotion [8–10].

Therefore, although there has been extensive development of fish-like robots capable of swimming, these previous systems cannot be expected to reproduce these walking gaits [11–14]. The gait of *P. senegalus* is also different from the gaits of other walking fishes [15–18]. For example, mudskippers use a 'crutching' gait which drives locomotion via the motion of pectoral fins without the articulation of the body axis [19], which has been demonstrated in several different robotic models [20–22]. Furthermore, bioinspired robotics have been used to create other types of terrestrial locomotion adjacent to the walking gait of *P. senegalus* such as the slithering of snakes [23, 24], the sprawling gait of salamanders [25, 26], and the peristaltic motion of worms [27, 28]. However, these other robotic models of locomotion are distinct from the combination of a single pair of anterior appendages and an articulating vertebral column characteristic of *P. senegalus*.

Modeling complex morphologies, such as those seen in animals, is a significant challenge in the development of bioinspired robots. Imaging technologies such as cineradiography [29], the combination of static CT scan images and dynamic x-ray video [30], and computer vision [31] can provide detailed data about the morphology and kinematics of an organism, but no robotic model can perfectly recreate the biological system of interest. Simplifications are necessary to create a physical instantiation and the level of detail required for the model depends on the research question to be answered [32]. For example, abstract models can be simple enough that their features are applicable to a range of disparate species, allowing researchers to contrast species throughout evolutionary lineages [33]. Abstracting away the majority of morphological details can produce a template that is applicable across a range of species while attempting to realistically replicate morphological details can produce a model anchored to the features of a specific species [34]. These simplified models can look like approximating a biped leg as an inverted pendulum with springs [35], simplifying a leg with many degrees of freedom to a single linkage [36], or creating a fish's tail actuated by tendons that leverages soft material properties to get specific spatial deformations with one actuator [37]. Furthermore, designing a system that generates net forward locomotion is nontrivial when considering nonidealized environments and uncertain contact points or ground reaction forces [38]. Several simulation and robotic studies have previously explored locomotion mechanisms similar to that of *P. senegalus*, including simplified body-limb coordination models and reconfigurable amphibious robots that emulate primitive tetrapod walking behavior [39, 40]. While these studies provide valuable insights into body-limb coordination and gait transitions, our work focuses on developing a minimalistic physical robot directly informed by the midline kinematics of *P. senegalus* during terrestrial locomotion.

In this work, we present a single-actuator wave-like continuum robot inspired by the walking fish *P. senegalus* (figure 1). This robot consists of fifteen rigid links actuated by a rotating helix such that the single rotational degree of freedom propagates an undulating wave down the body of the robot [41]. We augmented the robot with a single pair of fin-inspired appendages in the anterior portion of the body, using the undulating body wave to create a walking gait rather than a slithering or peristaltic gait.

To narrow the design space of infinite potential undulating body waves to biologically plausible motions, we generated four helical waveforms based on representative body postures tracked from experiments with *P. senegalus* specimens. We used each helix to actuate the robot and measured the forward walking speed of the robot's locomotion with each. Finally, we compared the kinematics of the robot with each helix to the body postures to assess how well a mechanism with a single degree of freedom reproduces the shape of the fish. While the fish-inspired robot does not replicate the kinematics of *P. senegalus* exactly, The results of this study indicate that, on smooth and flat ground, a slender-bodied robot with a pair of appendages can move forward using undulatory gaits that are simpler than those observed in real fish. Figure 2 provides an overview of the robot-twin framework, provides an overview of the robot-twin framework and summarizes how biological midline data from *P. senegalus* are translated into helix designs and subsequently evaluated through robotic experiments.

In section 2, we describe the experimental methods for collecting data from the *P. senegalus* specimens

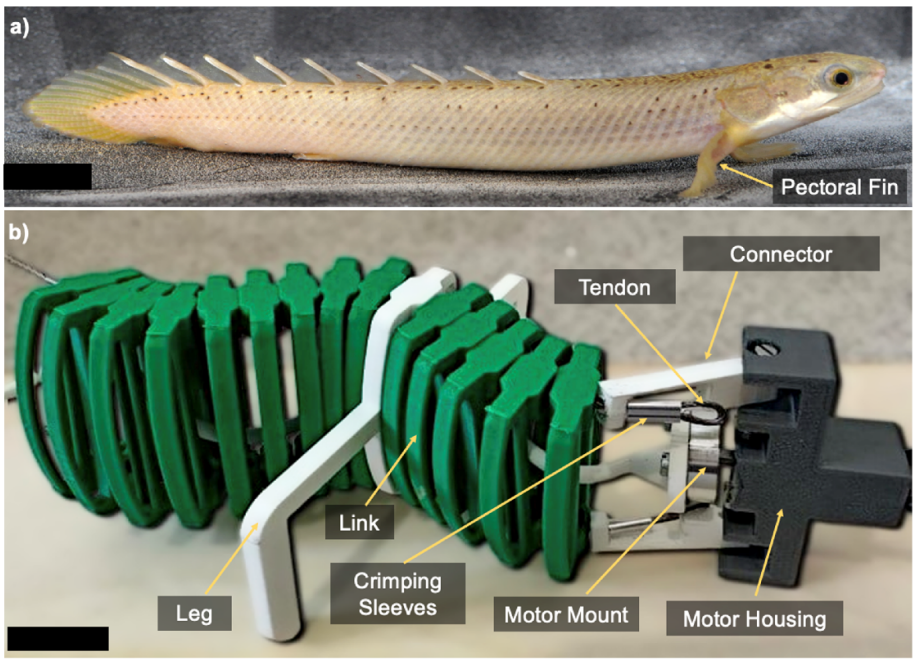

Figure 1. The robot and its biological inspiration (a) lateral view of *Polypterus senegalus* (scale bar for fish 10 mm). (b) Single-actuator wave-like robotic fish (scale bar for robot 15 mm).

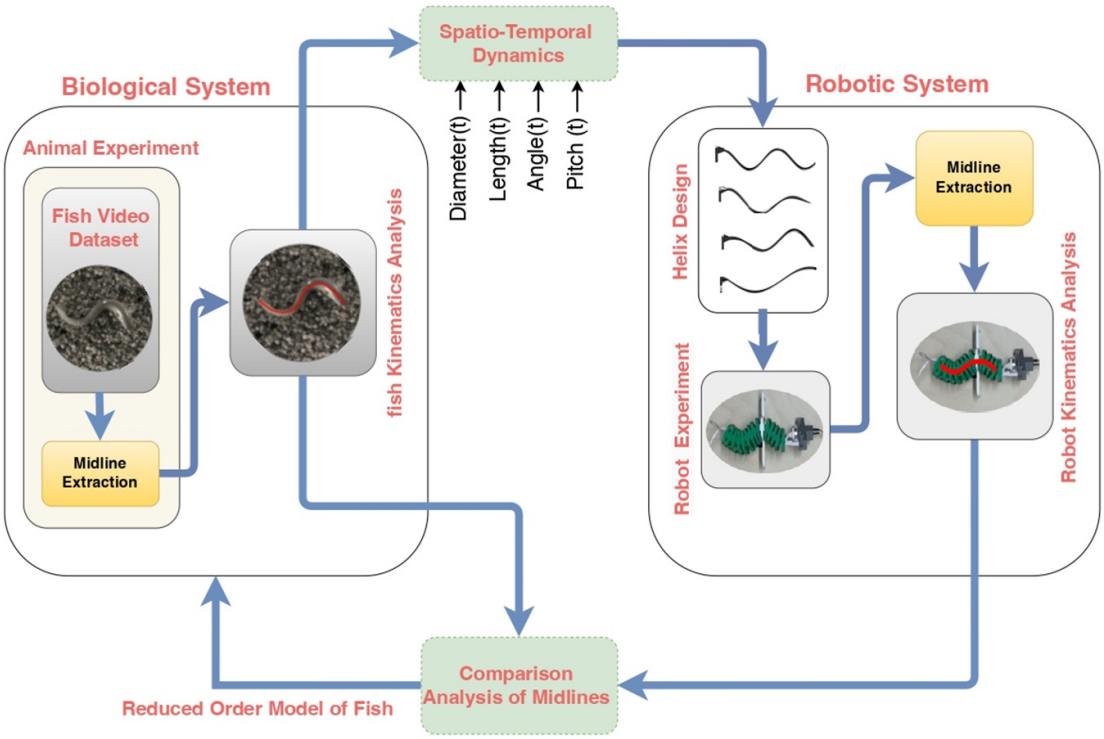

Figure 2. 'Robot-twin' pipeline. Biological kinematic data from *P. senegalus* were translated into the design of several distinct robotic models, which were then experimentally evaluated and compared to the fish to determine which reduced-order model best approximated the biological midline trajectories.

and the data processing pipeline for obtaining the kinematics of the fish. In section 3, we explain the design of the robot and how the kinematics of the fish are converted into the relevant design parameters. In section 4, we discuss the experimental characterization of the robot with different helix designs and in section 5, we compare the motion of the fish to the motion of the robot with different helices. Finally, we

present conclusions and future implications of this work in section 6.

2. Tracking the midline kinematics of *P. senegalus*

Analyzing the kinematics underlying animal locomotion is a natural first step to translate the movement of the biological inspiration to the design of a robot. Because the literature is sparse on the design of robots that utilize fish-like walking gaits, we collected data about the kinematics of *P. senegalus* to use as the basis of the walking motion of the robot. As such, we performed experiments with *P. senegalus* specimens and tracked the midlines of the individuals during terrestrial locomotion. Figure 3 presents the process of tracking the midline from dorsal view videos of the fish specimens via detection, segmentation, and skeletonization steps.

2.1. Recording walking kinematics of *P. senegalus*

Experiments were performed using five *P. senegalus* specimens with an average body length (BL) of 10.72 cm and average mass of 7.22 g. The fish were placed in a 28 cm × 18 cm fish tank that had medium-sized gravel covering the bottom to simulate natural terrestrial conditions (figure 3(a)).

A high-speed camera was positioned directly above the tank, capturing dorsal-view videos of fish locomotion at 250 frames per second in gray scale. To calibrate the video frames to absolute units, we also took videos of a static calibration object with thirty features of known dimensions so that the scaling and any linear or angular offsets of subsequent frames with the fish were known.

Five *P. senegalus* specimens were used in the experiments generating six locomotion trials between them. Capturing consistent locomotion data presented challenges, as the fish did not exhibit uniform walking behavior and exhibited intermittent movements with frequent pauses, and significant lateral deviations instead of steady, straight walking. The average recorded duration of each trial was approximately 30 s; however, usable segments within these recordings were limited due to inconsistent locomotor behavior. Therefore, five videos from five different individuals in which the fish walked in a consistent straight path for multiple steps were selected for analysis, where one gait cycle starts and ends with the tip of the fish's tail at its extreme position on the left side of the body (e.g. supplementary video S1). Figure 3(b) provides a series of representative example frames of the collected dataset which shows the fish's posture during a single gait cycle from the dorsal view.

2.2. Tracking the midline of *P. senegalus*

Figure 3(b) illustrates the complete automated pipeline used for extracting the fish midline using computer vision techniques. As a first step, all frames from the recorded video dataset were extracted and used as input images for the detection algorithm. The fish was initially detected using the grounding-DINO algorithm, a zero-shot detection model that utilizes text-based prompts to identify objects without requiring manual annotation [42]. A general descriptor prompt, 'fish', was provided to accurately locate the target object within each frame. Grounding-DINO returns tight bounding boxes around the detected fish, effectively eliminating the need for manual labeling, thereby streamlining the entire detection pipeline.

Following the detection of the fish, we then segmented the fish's body from the background using the segment anything model (SAM) [43]. SAM leverages the bounding boxes provided by grounding-DINO as initial prompts to generate pixel-level segmentation masks, effectively isolating the fish body from the gravel background to generate a binary mask. We then applied a skeletonization method to extract the midline of the shape, which reduced the binary object to its central pixels [44], in this case returning the midline of the fish from snout to tail. We used an existing algorithm (`skimage.morphology.skeletonize` Python library [45]) to extract a one-pixel-wide midline that captures the fish's body curvature. The initial skeletonized midline can appear jagged or contain small extraneous branches due to pixel-level noise in the segmentation mask, so we applied a low-pass filter to smooth the midline. The results of the entire tracking and midline extraction pipeline used in this study are illustrated in figure 3(b).

3. Design of the single-actuator wave-like robotic fish (SAWRF)

The SAWRF is made up of five main elements: a motor, a motor housing, a helix, a chain of fifteen rigid links that form the body of the robot, and a pair of legs (analogous to the pectoral fins that the fish uses in terrestrial locomotion). The single actuator of the SAWRF is a 50 rpm DC motor (mass of 10 g with 2.2 kg·cm locking torque). The helix is mounted directly to the motor output shaft so that as the motor spins, the continuous rotation of the helix induces a sinusoidal bending wave through the body (figure 4(a)). The links are connected to each other by flexible but inextensible 1.5 mm braided wire tendons that pass through from the motor housing to the final link. These tendons prevent the links from separating axially or from rolling with respect to each other. There is a small amount of slack in the tendon that allows the helix to create in-plane undulation while avoiding self-collisions between the tendons. The first link is attached to the motor housing and the sixth link is attached to a pair of small legs, which are longer than the height of the links(figure 4(b)).

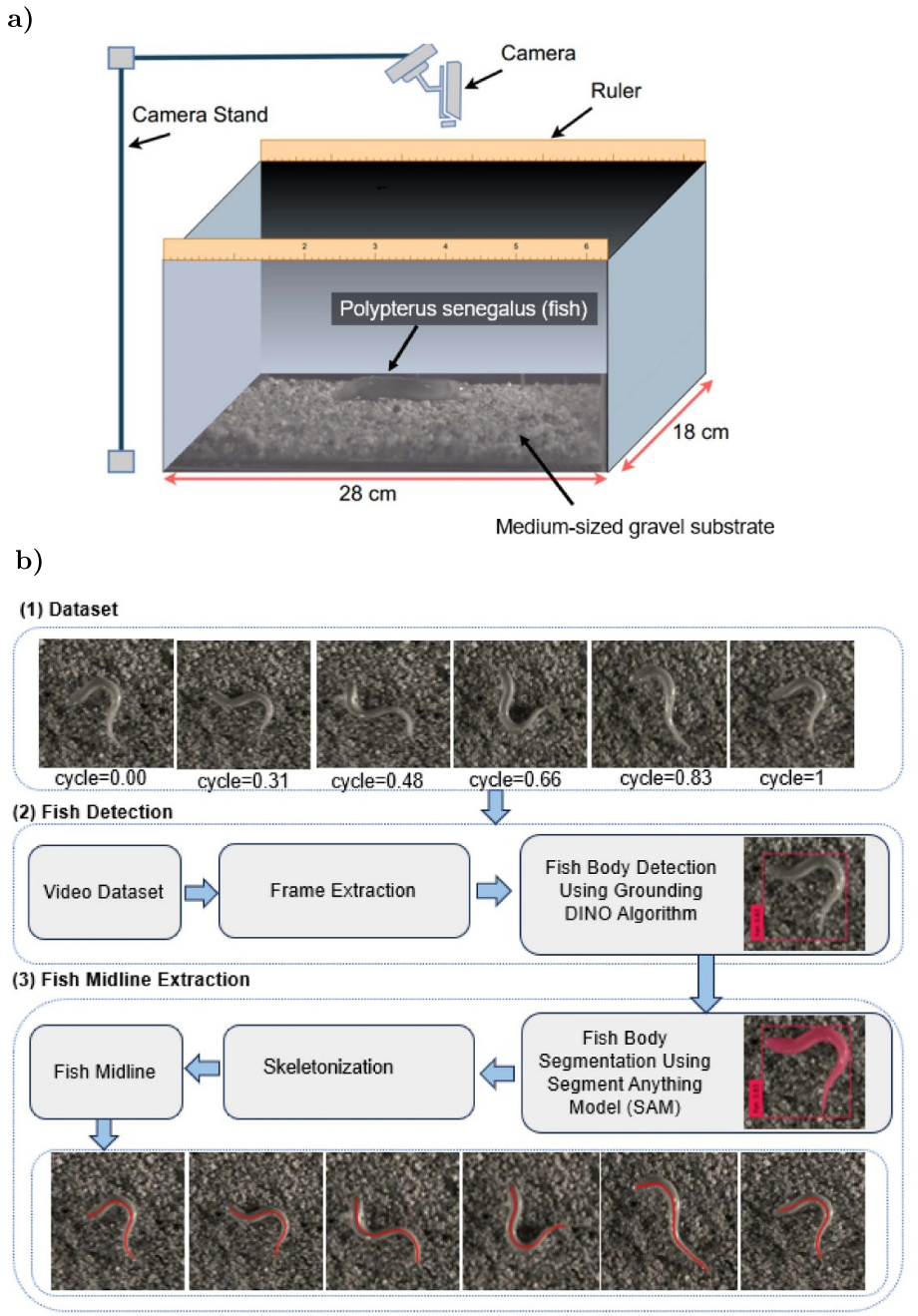

Figure 3. Capturing data from the *P. senegalus* specimens. (a) Experimental setup for fish locomotion tracking in which dorsal view videos of the fish on small gravel were obtained. (b) Pipeline for midline extraction: (1) dataset frames captured from dorsal-view videos of *P. senegalus*, (2) fish detection using grounding-DINO (3) fish body segmentation from background via segment anything model and midline extraction via skeletonization.

Figure 5 illustrates the internal configuration of the robotic fish at different rotations of the helix, demonstrating how the helix's motion alters the positions of the links and legs relative to each another. The BL can be adjusted by varying the number of links; however, beyond a certain number of links for a given helix length, the helix end is more likely to become trapped between the last links, which halts the motor's rotation. As the helix rotates, it creates an undulatory motion that propagates along the body links, generating the robot's forward movement. To highlight how the configuration evolves, three key links are displayed in color: the first link attached to the motor housing, the sixth link attached to the legs, and the final link. The remaining links are made transparent to visualize how the helix's interactions with the links changes the body's shape. Figure 5(a) illustrates the robot at the initial position which we define as 0° rotation. Figure 5(b) shows the robot configuration after the motor has rotated 90° clockwise and figure 5(c) illustrates the configuration after 180° rotation.

The shape of the robot's body continuously changes as a function of the geometry of the helix

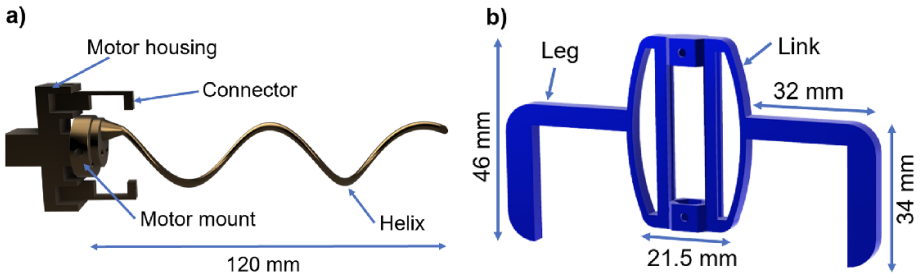

Figure 4. Structural components of the SAWRF. (a) The rotating helix system that consists of a motor housing, motor mount, and connector that produces the cyclical motion to generate undulation of the body. (b) Image of the body link with attached legs that contributes to generating ground reaction forces for forward locomotion.

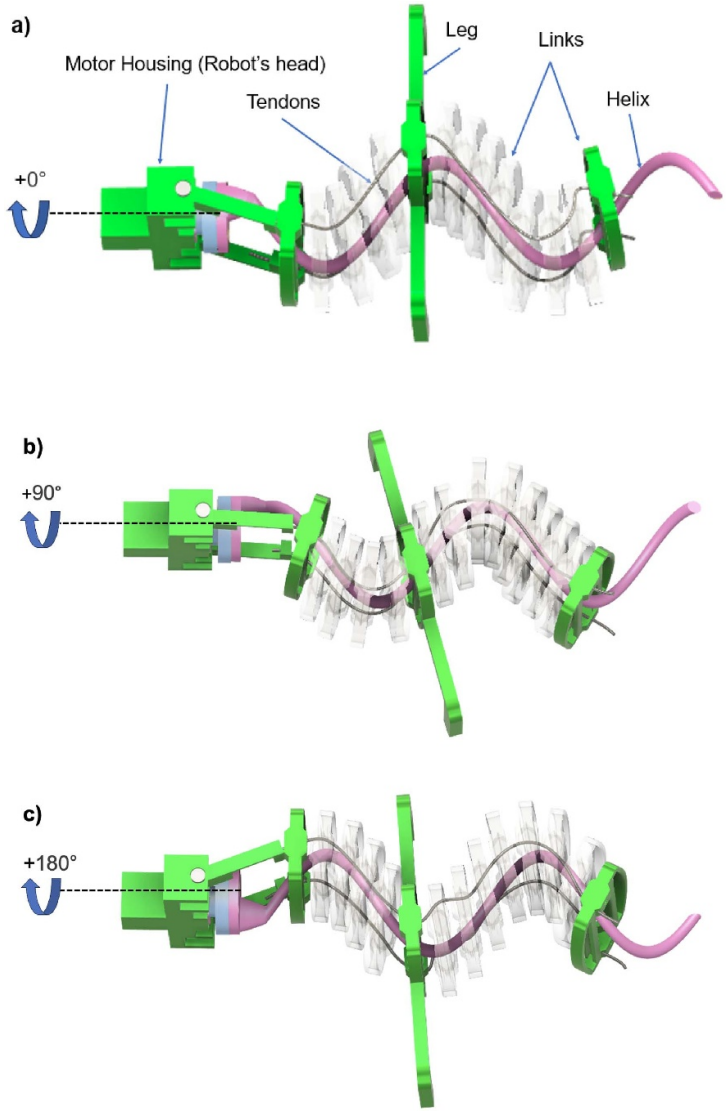

Figure 5. Sequential states of the single-actuator wave-like robotic fish (SAWRF) during helix rotation and relative positioning of the links, helix, and leg at different motor rotation angles. (a) Initial configuration at 0° rotation with a single bend in the center of the robot, (b) At 90° rotation, the helix-driven movement shifted the links and leg relative to each other into a shape with two bends. (c) At 180° rotation, with a single bend in the center of the robot in the opposite direction of the 0° shape.

and the angle of the helix's rotation. While there can be a small amount of uncontrolled motion between the links as a function of the tolerance between the sliding parts (tendon and links, links and links, links and helix), this shape change is negligible compared to the pattern of undulation defined by the helix shape. The friction between the tips of the legs and the ground transformed this oscillatory movement into forward thrust. The entire robot weighed 62 g and was 175 mm in length and 52 mm in height. The motor

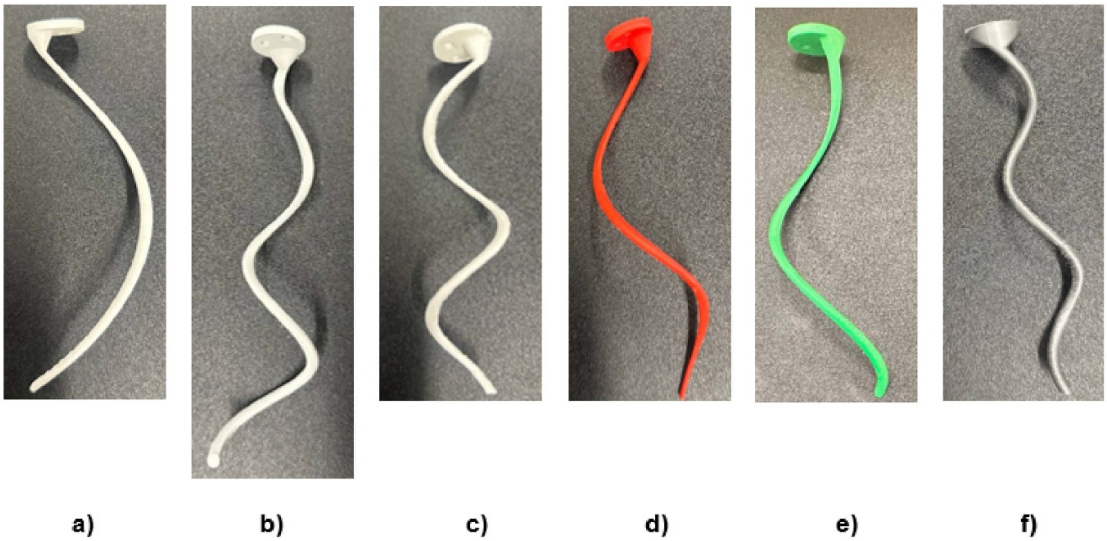

Figure 6. 3D-printed helix prototypes with varying geometric parameters. Each helix differs in diameter, pitch, height, and transition angle, affecting the wave propagation and locomotion characteristics of the robot. (a) $D = 40$ mm, $P = 157$ mm, $L = 110$ mm, $\theta = 0°$. (b) $D = 9.5$ mm, $P = 66.67$ mm, $L = 140$ mm, $\theta = 5°$. (c) $D = 25$ mm, $N = 2$, $P = 55$ mm, $L = 110$ mm, $\theta = 0°$. (d) $D = 20$ mm, $P = 91.67$ mm, $L = 110$ mm, $\theta = -4°$. (e) $D = 45$ mm, $P = 100$ mm, $L = 110$ mm, $\theta = 10°$. (f) $D = 16$ mm, $P = 61.11$ mm, $L = 110$ mm, $\theta = 0°$.

housing, legs, helix, and body links were 3D-printed from rigid PLA plastic. During all the experiments, the motor of the SAWRF was powered by an offboard power supply.

3.1. Design of the rotating helix

The helix plays a crucial role in the propulsion mechanism of the SAWRF because it determines the kinematics of the robot's body. The geometry of the helix defines how the fifteen links change position with respect to each other as a function of the helix's angle of rotation.

The helix is a circular coil defined by four primary parameters: diameter (D), pitch (P), transition angle (θ) and length (L). These 3D parameters uniquely define the curvature, amplitude, and wavelength of the 2D wave that propagates down the robot's body. Altering the helix parameters changes the robot's morphology and gait; for instance, varying the diameter of the helix affects the amplitude of the induced wave. Thus, we can design different helices that will generate desired body shapes of the robot to explore how the body kinematics affect locomotion speed of the robot or the fish. Figure 6 presents a set of 3D-printed helices with varying geometric parameters.

We define the four helix parameters as follows:

- **Length (L):** the total length of the helix, measured along its central axis (z-axis) from one end to the other. This determines the longitudinal span over which the wave propagates along the robot's body; the longer the helix, the longer the body of the robot will be, requiring either more links or thicker links.
- **Diameter (D):** the initial diameter (x–y plane) of the circular path followed by the helix around the axis. This parameter, along with the transition angle, defines the amplitude of the wave generated along the robot's body, where helices with larger diameters generate body waves with larger amplitudes, which may influence ground interaction and propulsion.
- **Pitch (P):** the axial distance between two consecutive turns of the helix. This determines the wavelength, with larger pitches producing longer wavelengths and affects the curvature of the motion.
- **Transition angle (θ):** the angular parameter that determines how the radius of the helix changes along its length. The value of the transition angle for each helix was determined from the change in amplitude observed along the extracted midline of the fish and was constrained by the maximum allowable amplitude within the robot structure. A transition angle of zero produces a wave with constant amplitude along its length. A positive transition angle increases amplitude along its length (i.e. the tail has a larger amplitude of oscillation than the head) and vice versa for a negative transition angle. This results in a non-uniform bending profile, where one part of the robot body exhibits larger curvature.

The design and evaluation of the helix shapes were informed by the midline kinematics of *P. senegalus*. Representative midlines extracted from dorsal-view videos were used as biological references to determine suitable geometric parameters for the helix. The selected parameters balanced the characteristic bending pattern observed in the fish with the mechanical constraints of the robot, including link spacing, tendon

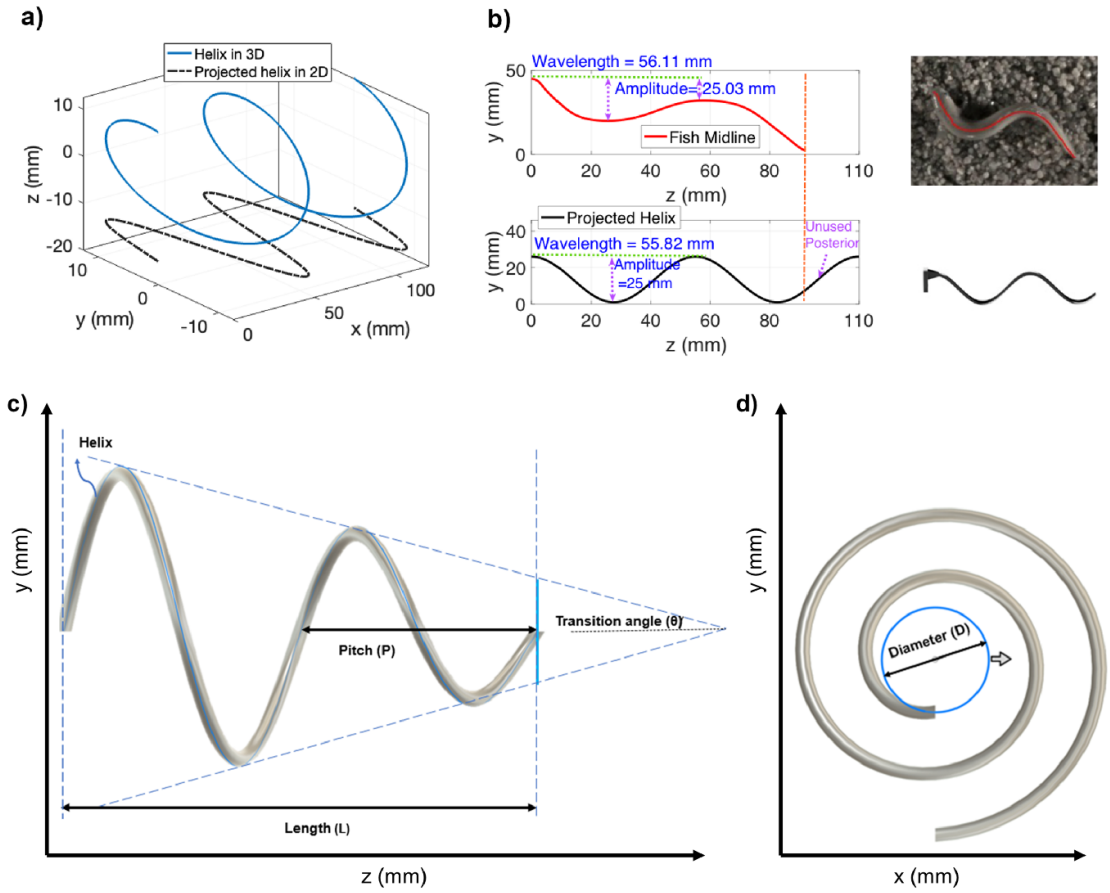

Figure 7. Translating the 2D midline of the fish to a 3D helix. (a) 3D representation of the helix with its corresponding 2D projection onto the x–y plane. The coordinate system is defined such that the z-axis corresponds to the longitudinal axis of the fish (head-tail direction), while the x- and y-axes define the lateral plane orthogonal to this axis. This projection is used to compare the helix geometry with the extracted midline of the fish. The geometric parameters of the illustrated helix are length (L) = 110 mm, diameter (D) = 25 mm, pitch (P) = 55 mm, and transition angle (θ) = 0°. (b) Quantitative comparison between the fish midline (red curve) and the projected helix wave (black curve). (c) Side-view schematic of generalized helix variables: pitch (P), length (L), and transition angle (θ). (d) Front-view schematic of helix variable diameter (D).

clearance, and the maximum height that could be accommodated inside the body. Each helix was then fabricated and evaluated experimentally to examine how its geometry influenced locomotion. The projected two-dimensional shapes of the helices were visually compared with the corresponding fish midlines to confirm similarity in amplitude and wavelength. The locomotion tests, performed under different motor input voltages, were used to assess how each design affected forward speed, stability, and lateral displacement.

We define the helix's trajectory in three-dimensional space using the following parametric equations:

$$\begin{aligned} x(\phi) &= \left(\frac{D}{2} + z(\phi)\tan(\theta)\right)\cos(\phi), \\ y(\phi) &= \left(\frac{D}{2} + z(\phi)\tan(\theta)\right)\sin(\phi), \\ z(\phi) &= \frac{P}{2\pi}\phi, \end{aligned} \tag{1}$$

where ϕ is the angular parameter (in radians) used to trace the helix, and varies from 0 to $\frac{2\pi L}{P}$. The helix is defined in a Cartesian coordinate system as illustrated in figure 7(a) where the z-axis corresponds to the longitudinal axis of the fish (head-tail direction) running along the center of the body, while the x- and y-axes define the lateral plane orthogonal to this axis. In this frame, the helix is wrapped around the z-axis, and its projection onto the x–y plane describes the lateral curvature of the wave. The parametric equations of the helix define this geometry, with $x(\phi)$ and $y(\phi)$ giving the lateral displacement and $z(\phi)$ describing the longitudinal progression along the body axis.

Increasing θ is constrained by the robot's internal geometry as the helix must be able to rotate inside the slots of the links. A larger transition angle or diameter may cause the helix to interfere with the inner walls of the links, limiting the helix's ability to rotate. Furthermore, to generate a feasible helix, the diameter and transition angle must be chosen such that $x(\phi)$ and $y(\phi)$ are always positive and the initial diameter is larger than the thickness of the helix.

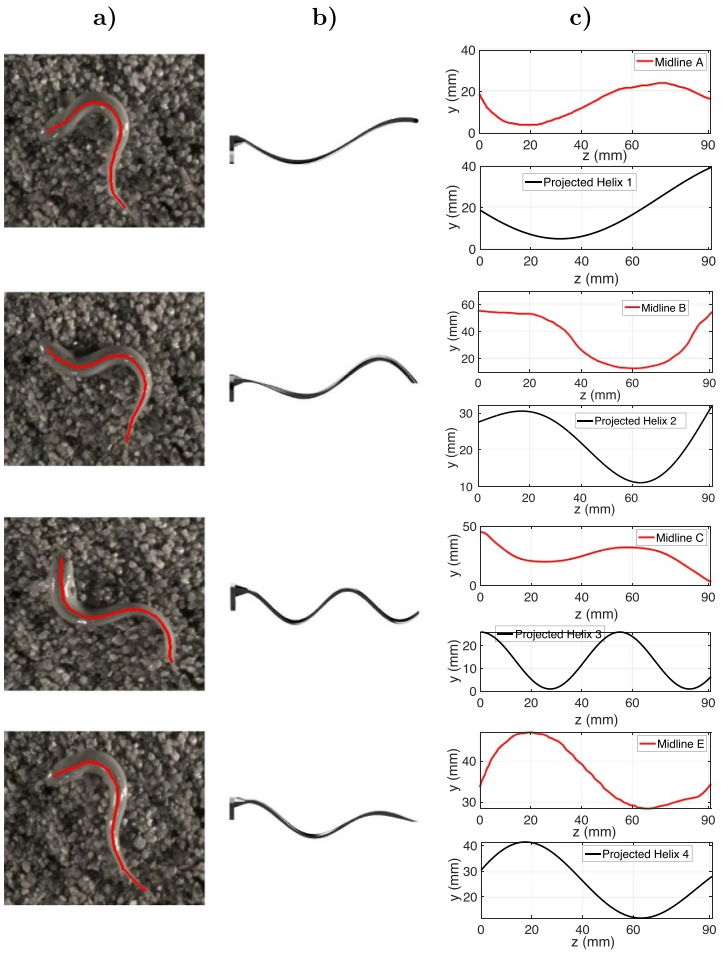

Figure 8. The four helices inspired by the midline of a *P. senegalus* specimen. (a) Frames of the fish used as reference for the helix designs with overlaid midlines. (b) CAD models of the four helix types, each with a fixed length of 110 mm. The parameters of each helix are as follows: Helix 1: $D = 40$ mm, $P = 157$ mm, $\theta = 0°$; Helix 2: $D = 45$ mm, $P = 100$ mm, $\theta = 10°$; Helix 3: $D = 25$ mm, $P = 55$ mm, $\theta = 0°$; Helix 4: $D = 20$ mm, $P = 91.67$ mm, $\theta = -4°$. (c) Comparison of the 2D projections of Helix 1, Helix 2, Helix 3, and Helix 4 with their corresponding midlines, showing the similarity in amplitude and wavelength.

We designed four helices with curvature profiles inspired by representative examples of the fish's midline at different timesteps of their gait cycles.

All helices were constrained to a thickness of 3.5 mm, a fixed total length of 110 mm, a maximum amplitude of 25 mm matching the height of the central slot in each link (i.e. maximum values of both $x(\phi)$ and $y(\phi)$ were 25 mm), and a minimum pitch of 55 mm to ensure that the resulting body curvature did not exceed the bending angles observed in the fish. For each design, we projected the 3D helix into 2D space to directly compare the planar shape of the robot with the planar view of the fish in terms of amplitude and wavelength of the body wave. The projection onto the x–y plane describes the wave that propagates down the length of the robot.

Figure 7 shows the design and evaluation process for one of the helices with a diameter of 25 mm, a pitch of 55 mm, and a transition angle of 0°. Figure 7(b) presents a quantitative comparison between the extracted midline of one frame of *P. senegalus* and the 2D projection of the designed helix. The midline of the fish is approximated by a sinusoid of wavelength 55.15 mm and amplitude 25.03 mm, and the projected helix wave has a similar wavelength of 57.4 mm and amplitude of 25 mm. The unused posterior section refers to the end portion of the helix that is not covered by the body links. Figure 7(c) further illustrates the geometric variables of the helix: pitch (P), length (L), and transition angle (θ) in relation to the projected body wave, while figure 7(d) provides a top down view of the helix highlighting the definition of its diameter (D). These visualizations clarify how each parameter contributes to shaping the robot's body curvature and wave propagation.

Figure 8 compares the four helix designs inspired by the midline patterns of *P. senegalus* we generated for the robotic system. Figure 8(a) shows frames from experimental data with the extracted midlines of the real fish overlaid to highlight the oscillatory wave-like motion used as a reference for the designs of the helices.

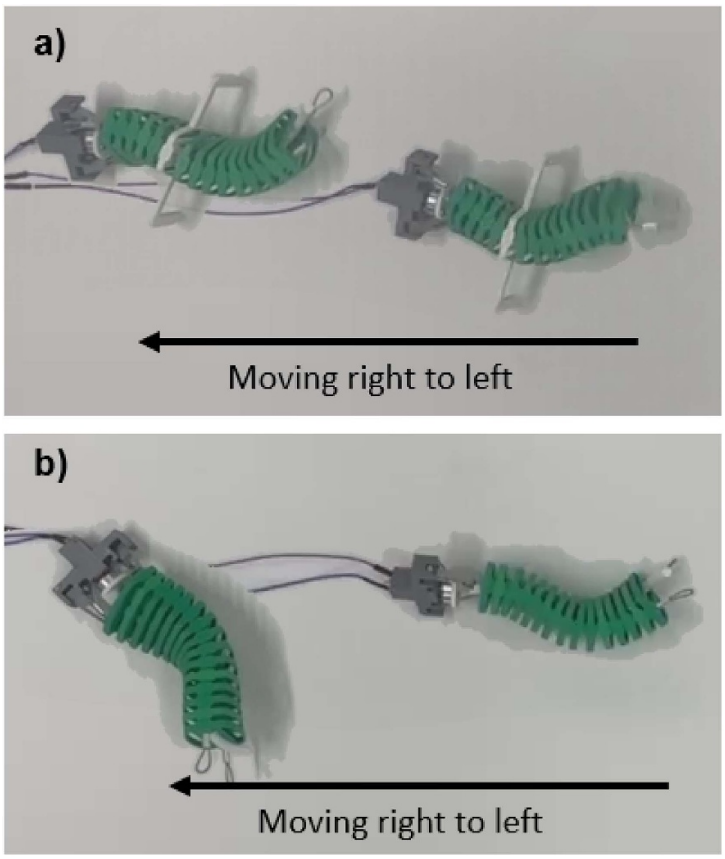

Figure 9. Comparison of the robot's stability with and without legs. (a) The robot with legs maintained its balance and forward movement. (b) The robot without legs exhibited instability in the roll axis and could not balance upright.

To capture variations in the fish midline, four helix designs were developed to generate sinusoidal waves spanning key geometric differences across the design space. Helix Type 1 (diameter 40 mm, pitch 157 mm, transition angle 0°) represents a posture with constant bending amplitude and low curvature. Helix Type 2 (diameter 45 mm, pitch 100 mm, transition angle 10°) produces undulation with amplitude increasing from head to tail. Helix 2 has a larger amplitude, a shorter wavelength, and more wave cycles along its length than Helix 1, and this leads to a more frequent undulatory pattern along the body. Helix Type 3 (diameter 25 mm, pitch 55 mm, transition angle 0°) corresponds to a posture where more than one wavelength is formed along the body with constant amplitude. Helix Type 4 (diameter 20 mm, pitch 91.67 mm, transition angle −4°) generates undulation with amplitude decreasing from head to tail. Figure 8(c) presents the two-dimensional projections of the helices and their corresponding fish midlines for all four designs, similar to the comparison shown in figure 7(b). This view highlights the similarity in amplitude and wavelength between the projected helix geometry and the extracted fish midline, demonstrating how each helix shape was derived from the biological reference.

3.2. Leg design

The robotic fish also has two passive legs inspired by the pectoral fins of *P. senegalus* [7, 46], which are attached to the sixth body link at a point that slightly elevates the body off the ground. This elevation reduces surface friction and contributes to overall stability during locomotion.The leg geometry was refined through a series of experimental trials to achieve stable and consistent forward walking performance. Since the leg dimensions influence body elevation, stability, and actuation load, different prototypes were tested to identify a functional range. Legs shorter than the link height were insufficient to lift the body and resulted in loss of balance, whereas longer legs caused the robot to tip during locomotion. Increasing the leg mass beyond the tested range added load to the motor, reducing its ability to maintain smooth forward motion. These observations guided the selection of a leg length slightly greater than the body link height, which provided sufficient body elevation and stability during walking without increasing the actuation effort.

Figure 9 presents the motion of the robot actuated with Helix 2 at 0.75 Hz for two configurations: figure 9(a) with legs and figure 9(b) without legs attached. The robot with legs was operated for

approximately 24 s, and the robot without legs was operated for 27 s.

If the robot does not have legs attached, when the undulation of the body causes some rotation around the roll axis, the center of mass shifts outside the contact points where the links touch the ground and the robot cannot maintain balance. However, if the robot has legs, the support polygon formed by these new contact points with the ground is wider and the center of mass remains above the support polygon so the robot can maintain its upright orientation. This shows that passive legs are sufficient to prevent the robot from rolling over as the helix creates large-amplitude waves down the body (supplementary video S2). Through experimentation, we tested various leg positions along the body links and identified a placement at the sixth link from the motor housing where the robot consistently exhibited forward motion rather than lateral motion. The legs were designed as simple rigid structures inspired by the pectoral fins while maintaining robustness and ease of fabrication. Their lengths were set slightly longer than that of the body links so that the body could be lifted during locomotion, and the height was determined experimentally by testing several prototypes to identify a configuration that produced reliable forward motion.

4. Experimental setup and results

To evaluate the locomotion performance of the SAWRF, we conducted a series of experiments to measure the robot's speed and analyze the kinematics of its body to compare its movement patterns with those of *P. senegalus*. We recorded videos of the robot's motion with different helices to assess how the undulatory motion driven by the helix influences forward speed, lateral oscillations, and body curvature (supplementary videos S3–S6).

We then compared the experimental results from the robotic fish to locomotion data from *P. senegalus* to evaluate the similarities of locomotion generated by the various helices. This analysis helps assess how closely the robotic movement aligns with biological locomotion and offers insights for optimizing helix parameters to improve robotic mobility in future designs.

4.1. Experimental setup

We evaluated the locomotion performance of the robotic fish by operating it on a flat wooden board. The robot was tethered to an external DC power supply that provided an adjustable input voltage to the motor. We recorded the motion of the robot via a fixed overhead 12-megapixel camera.

4.2. Experimental results

To evaluate how helix morphology influences locomotion, we analyzed the gait patterns of the SAWRF using the four different helix designs shown in figure 8(b). Figure 10 shows timeseries images and overlaid midlines of *P. senegalus* and the robot with each of the four helices. Figure 10(a) presents images of five representative midlines of the fish, corresponding to time points of 0.00, 0.31, 0.48, 0.66, and 0.83 of the gait cycle. These extracted midlines form the basis of the helices' geometries. Figures 10(b)–(e) illustrate the gaits of the robotic fish equipped with each of the four helices. For each case, the robot's body posture is captured at gait fractions of 0.00, 0.20, 0.40, 0.60, and 0.80. The representative frames of the fish and the robot were selected from each cycle to capture characteristic postural transitions, such as mid-bend, full extension, and body undulation. This approach allows for a meaningful qualitative comparison of typical body deformations despite differences in temporal alignment. These experiments were conducted with the robot actuated at a motor input frequency of 1 Hz. The midlines of the robot were extracted from video data using a YOLOv11-based detection and segmentation model [47] and a skeletonization algorithm similar to the method described in section 2.2.

Five representative midlines of *P. senegalus* (labeled A-E) were extracted at evenly spaced intervals over a complete gait cycle to capture the range of postures exhibited by the fish. From these, four midlines displaying distinct bending patterns were selected to inform the helix designs. Helix 1 was derived from Midline A, reflecting generally lower curvature throughout the body; Helix 2 was based on Midline B, which features high curvature in the middle of the body; Helix 3 was inspired by Midline C, characterized by a symmetric body shape; Helix 4 corresponded to Midline E, showing high curvature near the tail.

Figure 11 presents experimental results evaluating the locomotion performance of the robotic fish under four distinct helix designs (Helix 1–4) across motor input frequencies of 0.617 Hz, 0.75 Hz, 0.9 Hz, and 1.083 Hz. The tested frequencies (0.617 Hz, 0.75 Hz, 0.9 Hz, and 1.083 Hz) were generated by evenly spaced applied voltages within the operating range of the motor to examine the effect of actuation rate on locomotion performance. These frequencies are lower than those observed in *P. senegalus* due to mechanical constraints of the motor and link design, but in both the robot and the fish, forward velocity increased with actuation frequency, showing a comparable kinematic trend despite the difference in absolute values.

Figure 11(a) shows the forward velocity of the robot expressed in BLs per second (BL s^{-1}), where the robot's BL is 17.5 cm. Helix 4 achieves the highest forward speeds across all tested motor frequencies. Helix 2 and Helix 3 exhibit intermediate velocities, whereas Helix 1 consistently reaches lower speeds, showing minimal sensitivity to increasing motor frequency.

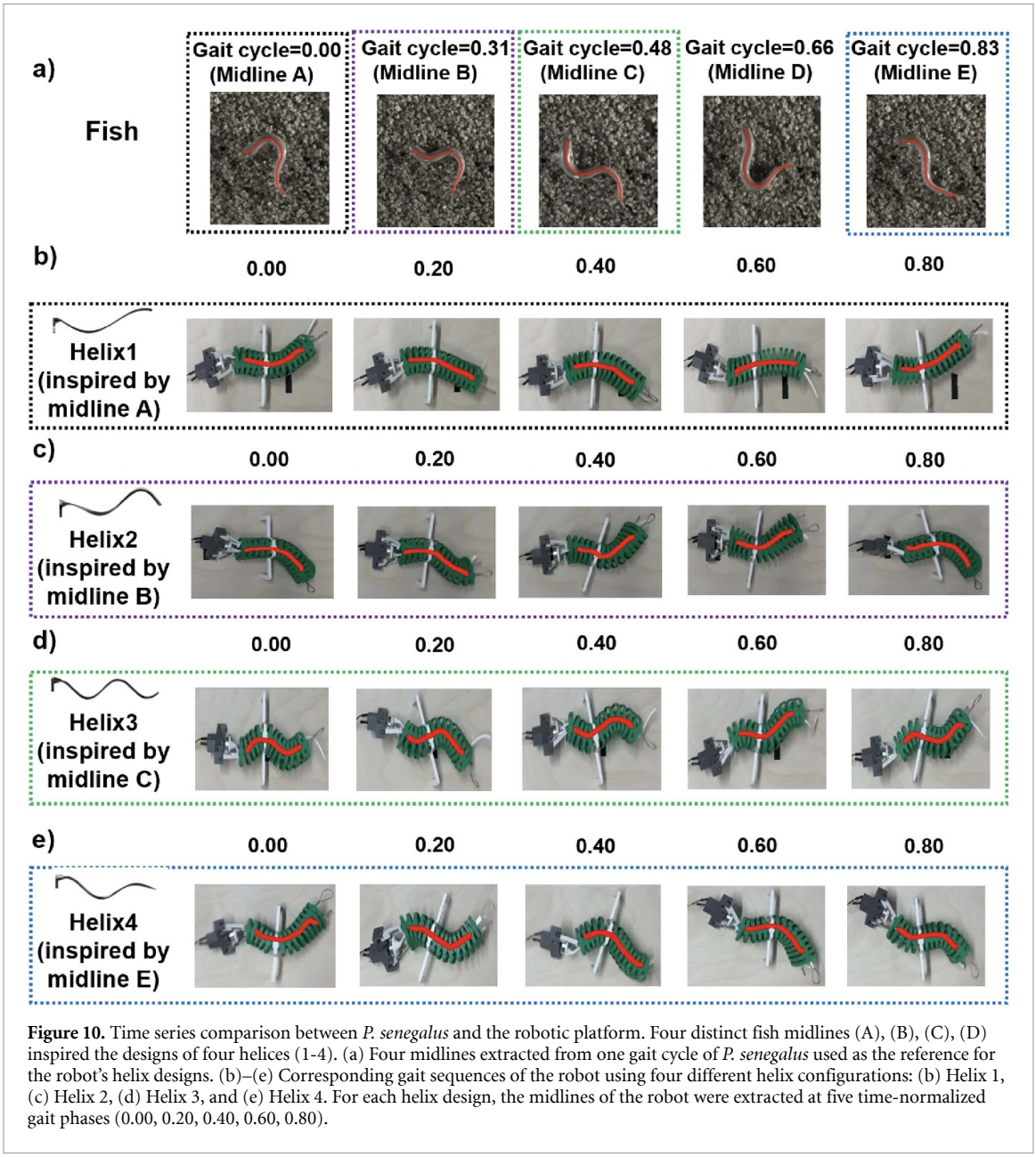

Figure 10. Time series comparison between *P. senegalus* and the robotic platform. Four distinct fish midlines (A), (B), (C), (D) inspired the designs of four helices (1-4). (a) Four midlines extracted from one gait cycle of *P. senegalus* used as the reference for the robot's helix designs. (b)–(e) Corresponding gait sequences of the robot using four different helix configurations: (b) Helix 1, (c) Helix 2, (d) Helix 3, and (e) Helix 4. For each helix design, the midlines of the robot were extracted at five time-normalized gait phases (0.00, 0.20, 0.40, 0.60, 0.80).

The trajectory of the head position of *P. senegalus* during terrestrial locomotion within the experimental tank is illustrated in figure 11(b). The fish displays significant lateral displacement, indicating a naturally oscillatory gait pattern rather than purely straight motion.

Figure 11(c) shows the head trajectories of the robot actuated at 1 Hz for 10 s with each helix design. Each helix configuration produces a distinct lateral displacement pattern characterized by varying degrees of side-to-side oscillation. Here, μ denotes the mean lateral displacement in y, the direction orthogonal to the intended direction of walking, and σ denotes the standard deviation of the lateral displacement. Helix 2 shows the smallest lateral deviation ($\mu = 0.0585$, $\sigma = 0.0373$), reflecting relatively stable forward motion with minimal lateral displacement. In contrast, Helix 1 exhibits the largest lateral displacement ($\mu = 0.1074$, $\sigma = 0.0700$), closely mirroring the pronounced side-to-side oscillations observed in the fish trajectory. Similarly, Helix 3 demonstrates significant lateral displacement ($\mu = 0.1053$, $\sigma = 0.0599$), while Helix 4 shows intermediate values ($\mu = 0.0778$, $\sigma = 0.0416$), indicating moderate lateral oscillation combined with stable forward progression. The variations in speed and lateral displacement shown here highlight how changes in helix geometry significantly influence the robot's stability, directional control, and locomotion efficiency.

5. Comparison of body kinematics between *P. senegalus* and the SAWRF

In this work, we have simplified the dynamic midline kinematics of *P. senegalus* to implement on a robot with a single degree of freedom that defines its

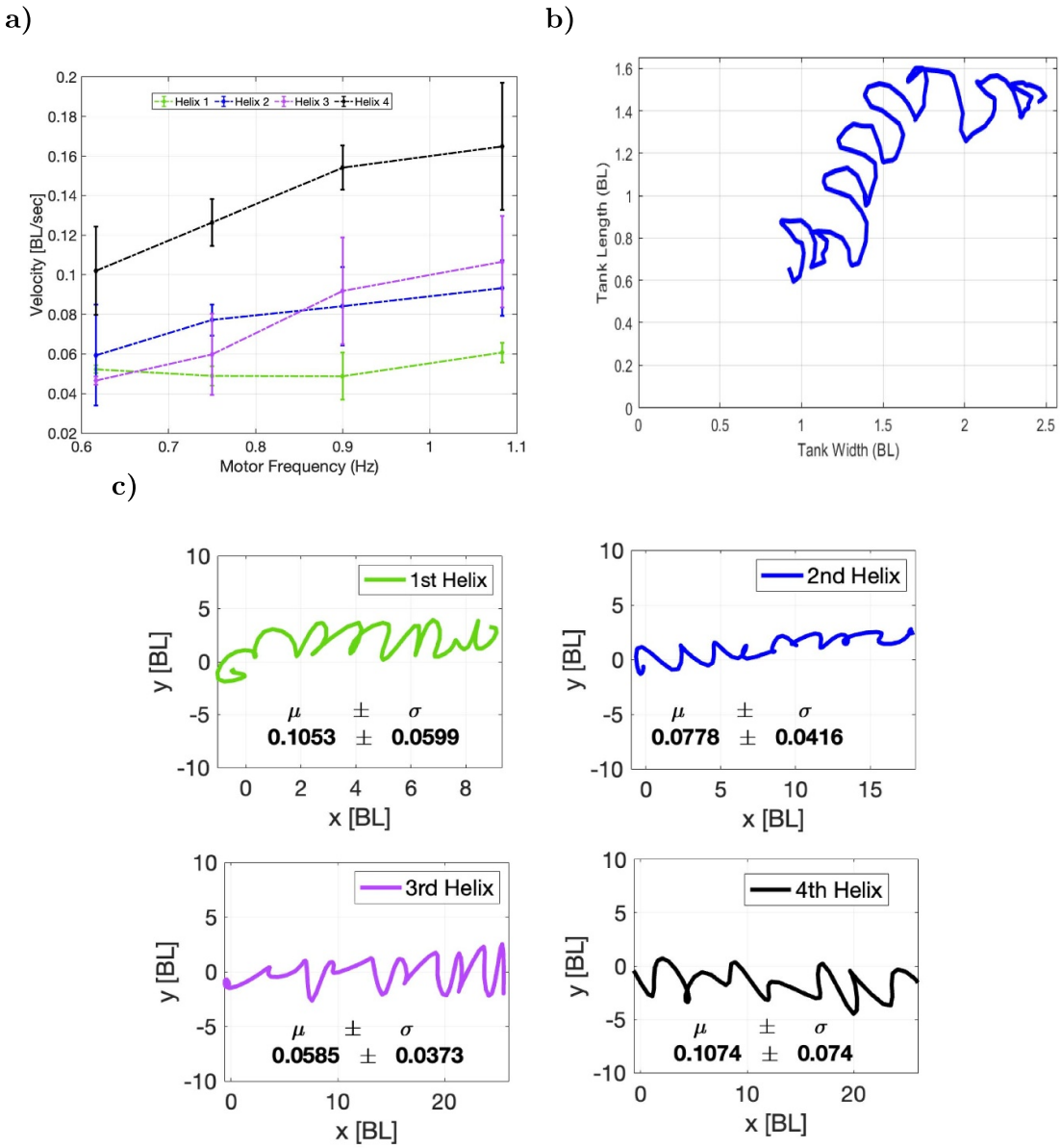

Figure 11. Speed and trajectory of the robot with the four helices compared with the trajectory of *P. senegalus*. (a) Average forward velocity of the robot with the four helix designs at varying motor frequencies. (b) Trajectory of the head position of *P. senegalus* during terrestrial locomotion on gravel substrate. (c) Trajectories of the robot head position showing lateral displacement across four different helix designs on a wooden plate. μ denotes the average y position of the robot (orthogonal to the intended direction of walking) and σ denotes the standard deviation of the y position.

body kinematics. The rotating helix creates a traveling wave down the body of the robot, but unlike the real fish, the properties of this wave are not time-varying. To assess the effectiveness of this simplified robotic model in mimicking the kinematics of the fish, we compared the midline of the robot with different helices to the midline of the fish at different timesteps throughout its gait.

5.1. Comparing kinematics based on midline similarity

We extracted five representative fish midlines (Midline A–E) from distinct timesteps within a complete gait cycle (figure 10(a)). We also extracted five midlines at evenly spaced timesteps from trials of the robot with each of the four helices (figures 10(b)–(e)), enabling a direct frame-by-frame comparison with the fish midlines. Figure 12 shows an example of this comparison, presenting an overlay of Fish Midline B (gait phase 0.66) with the midlines of the robot actuated using each of the four helix designs, captured at gait cycle phase 0.60. This visual overlay highlights differences in curvature between the biological and robotic midlines, which are quantified using RMSE (Root Mean Square Error) in figure 13.

To normalize the midlines of the fish and robot on the same scale for comparison, we first rotated both, aligning their long axes, and translated them so that both of their tail endpoints coincided in pixel space. The longitudinal axis of the fish midline was defined

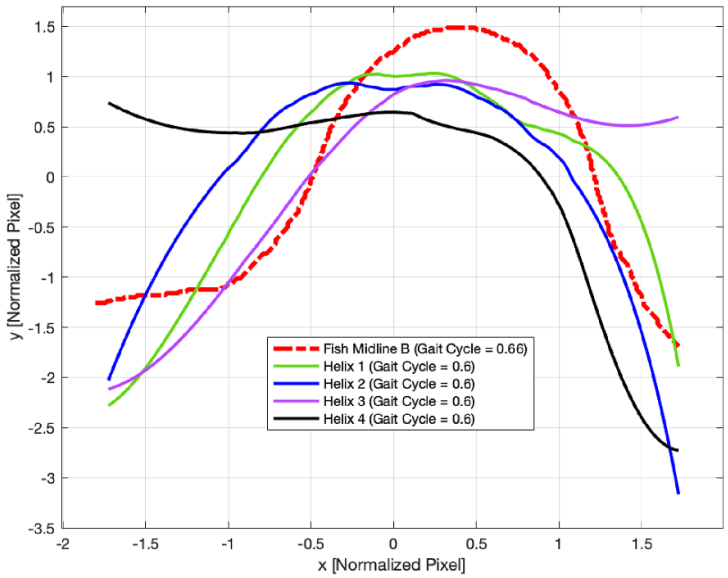

Figure 12. Comparison of *Polypterus senegalus*'s midline B at 66% gait cycle with the midlines of the robot generated using the four helices at 60% gait cycle. All midlines were spatially normalized and aligned so that they started and ended at the same x-position in the plot to enable direct geometric comparison. The RMSE comparison of fish Midline B with the robot midlines generated by Helix 1, Helix 2, Helix 3, and Helix 4 indicates that Helix 2 exhibits the lowest RMSE at 60% of the gait cycle (0.5069), compared to 0.5909, 1.5393, and 1.5265 for Helices 1, 3, and 4, respectively. This result shows that Helix 2 provides the closest geometric match to Midline B at this phase of the gait cycle.

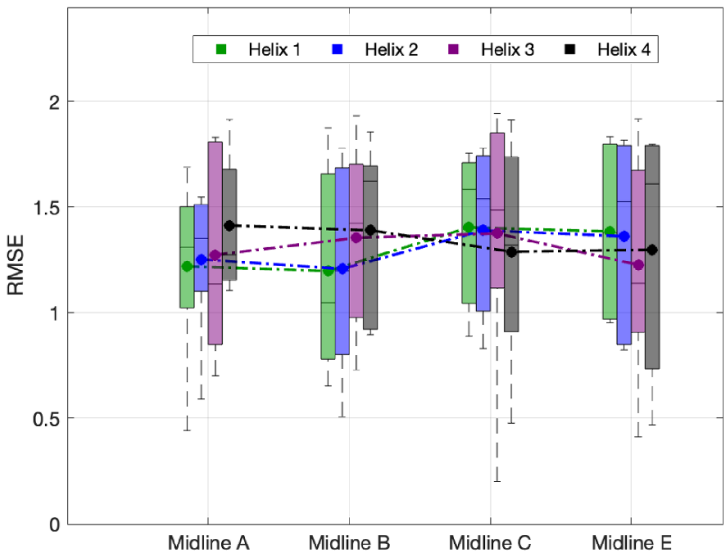

Figure 13. Root Mean Square Error (RMSE) values comparing midlines of the robotic fish driven by the four helix configurations with midlines extracted from four representative gait phases of *P. senegalus* (Midlines A, B, C, E). Each fish midline corresponds to a single frame of the fish's gait cycle and was compared against five evenly spaced timesteps of the robot gait cycle for each helix configuration. Each boxplot represents the distribution of RMSE values across these five robot timesteps, with mean values indicated by colored circles. Lower RMSE values correspond to closer geometric alignment between robotic and biological midlines. Helix 1 yielded the lowest mean RMSE when compared with Midline B, indicating the closest match in curvature at that gait phase.

by connecting the head and tail points extracted from the skeletonized midline. This line was used as a reference for aligning and rotating the midlines so that the body axis was parallel to the *x*-axis before comparison with the robotic midlines.Then, we linearly scaled the y coordinates of the robot's midline within the range of minimum and maximum coordinates of the fish's midline. To scale the horizontal axis of the robot's midline, we generated a vector of equally spaced x coordinates (the same number of points as contained in the fish's midline) within the minimum and maximum coordinates of the fish's midline. Finally, we used a cubic spline interpolation of the points previously generated by the normalization of the height to fit the robot's midline across the new range of x coordinates.

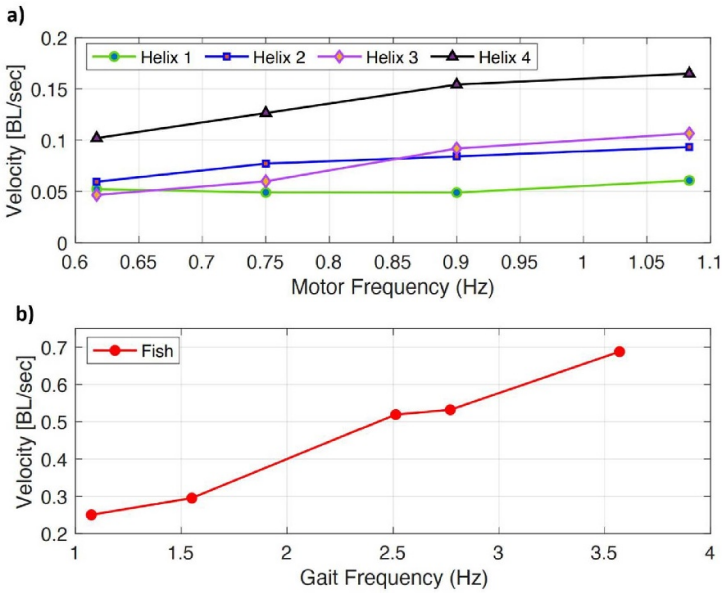

Figure 14. Comparison of the robot's walking speed and the fish's walking speed across different frequencies measured in body lengths per second. (a) Velocity of the robotic fish using different helix types at motor frequencies of 0.6, 0.75, 0.9, and 1 Hz. Helix 4 consistently achieved the highest speed across all motor frequencies. (b) Velocity of *P. senegalus* during terrestrial walking on gravel substrate measured across five individuals at gait frequencies from 1.1–3.57 Hz. The fish reached a peak velocity of 0.688 BL s^{-1} at 3.57 Hz.

Each RMSE value was then obtained by comparing a fish midline extracted from a single video frame with a robot midline taken from a single frame of the robot gait cycle under one of the four helix configurations (Helix 1–4). Five robot frames were sampled at evenly spaced points across one gait cycle for each helix, yielding five RMSE values for each fish-helix pair. Z-scores were calculated for each midline, defined as $z_i = (y_i - \mu)/\sigma$, where μ is the mean of all points on the midline and σ is the standard deviation of all points on the same midline. RMSE was then computed point-wise between the normalized fish and robot midlines. The resulting five RMSE values for each helix were aggregated into the distributions shown in figure 13.

Each boxplot in figure 13 summarizes the RMSE distribution across the five timesteps for each fish midline, providing a measure of the average spatial deviation between the robotic and biological midlines (e.g. the leftmost boxplot aggregates the deviations between the robot with Helix 1 at five timesteps and the snapshot of *P. senegalus* labeled Midline A). Midline B exhibited the lowest deviation with Helix 2 at 60% of the gait cycle (RMSE = 0.5069), compared to 0.5909, 1.5393, and 1.5265 for Helices 1, 3, and 4, respectively.

When we compare the robot's motion with each individual helix to the four midlines identified from the fish (i.e. comparing the effect of the helix design to the fish throughout the fish's gait cycle), we do not see significant statistical differences. This suggests that no single helix will consistently match the fish's kinematics throughout the entire gait cycle. However, all of the helices designed based on single snapshots of the fish's walking gait generate forward walking, indicating that the time-varying sinusoidal pattern is not necessary for this type of locomotion.

5.2. Comparing locomotion speed across frequencies

To evaluate how the robot's locomotion performance compares with that of *P. senegalus*, we measured the forward speed of both systems in units of BLs per second (BL s^{-1}). Figure 14(a) shows the velocity of the robot (17.5 cm in length) with four helix configurations across motor actuation frequencies of 0.6, 0.75, 0.9, and 1.1 Hz. Figure 14(b) presents the locomotion speeds of five trials of *P. senegalus* specimens (on average 10.9 cm in length) walking on a gravel substrate, measured across gait frequencies ranging from 1 Hz to 3.57 Hz. Both the fish and the robot exhibit faster walking speeds with higher frequency of their body undulations. The fish reaches a peak velocity of approximately 0.688 BL s^{-1} at a gait frequency of 3.57 Hz, while the robot with Helix 4 achieves the highest robot speed of approximately 0.18 BL s^{-1} at 1.1 Hz.

We observe that while both the fish and the robot walk faster with higher gait frequencies, the speed of the robot remains below that of the fish. This highlights the limitations of the single actuator in replicating the full biological motion. It also emphasizes the importance of other biological adaptations such as fin coordination and compliant structures that are not fully replicated in the current robotic design. Nonetheless, through this robot-twin framework, the

comparison offers insights into which aspects of the biological system contribute to more efficient locomotion and identifies areas where robotic implementation could be improved.

6. Discussion and conclusions

This study introduced a novel single-actuator wave-like continuum robot inspired by the terrestrial walking motion of *P. senegalus*. The robot consisted of a single motor and a rotating helix that actuates fifteen body elements, including a pair of appendages inspired by the fish's pectoral fins. The rotating helix, designed based on observations of the real fish's midlines, created a wave down the robot's body mimicking the spinal articulation of the fish. This work demonstrates that a minimalistic, single-actuator robotic fish can produce forward locomotion via simple axial undulation and additional ground contact with a pair of appendages. The constant sinusoidal wave generated by the rotation of the helix is simpler than the undulation observed in *P. senegalus*, suggesting that, within the context of smooth, flat ground locomotion tested in this study, closely replicating the fish's kinematics is not required to achieve effective movement. Nonetheless, other aspects of fish motion, such as body lifting, may become important on uneven or wet terrain or for improving energy efficiency.

A key methodological contribution of this study is the direct integration of biological data with mechanical design. Midline tracking of *P. senegalus* provided critical insights into body curvature and spatiotemporal dynamics, which were used to inform the parameterization of the helix geometry. We found that because the midline of *P. senegalus* is highly dynamic, no single constant sinusoid applied to the robot's body can closely match the undulation of the fish. Furthermore, the flexibility of the fish's body enables it to generate large curvatures not possible to generate in a robot with fifteen rigid links. In this work, mechanical constraints such as the fixed BL of the robot and the maximum achievable amplitude of the projected curve prevented us from generating helices closely matching certain postures of the fish. These limitations illustrate the classic tradeoff in bioinspired robotics of balancing adherence to specific features of the biological inspiration with the limits of a simple explainable model. However, our data-driven approach that converts observations of the biological organism to a simple robotic model demonstrates how a data-driven pipeline can be used to inform the design of a robot in cases where design intuition is not yet developed.

Our experimental results indicate that the parameters defining the body undulation have a significant impact on the locomotion of the robot. Helix 4, which creates more bending at the head of the robot than the tail of the robot, consistently demonstrated the highest forward velocity across tested input frequencies. However, this speed advantage came at the cost of greater lateral oscillation and less consistent directional stability. In contrast, Helix 3, the only helix that formed more than one complete wavelength along the body of the robot, achieved lower speeds than Helix 4 but produced the lowest side-to-side displacement of all the helices, which might be better suited for tasks requiring directional accuracy.

Among the four helix designs, Helix 3 produced the most consistent movement and exhibited the least lateral displacement in the robot's trajectory. However, this configuration was also the least representative of the fish's actual midline postures. In contrast, the midlines corresponding to Helices 1, 2, and 4 incorporated greater curvature and resulted in larger lateral displacements, more closely matching the body kinematics observed in *P. senegalus*.

The incorporation of simple paired appendages played a pivotal role in enhancing locomotion stability. While *P. senegalus* can twist its body to keep its center of mass over its body and pectoral fins, this one degree of freedom robot cannot bend out of plane to keep its balance during walking. The robot's appendages prevented it from rolling by maintaining ground contact throughout the gait cycle and widening the area of its support polygon. This passive mechanical solution contributed to upright body posture without introducing additional actuation complexity, demonstrating a practical compromise between functionality and simplicity. The use of a constant-shape helix to generate wave propagation offered both advantages and limitations. It allowed for precise and repeatable control using a single actuator, significantly reducing mechanical and computational overhead. However, the robot lacked the ability to change its body shape dynamically throughout the gait. As such, although our helix-based designs approximate certain kinematic features of the fish, they remain constrained by their fixed geometry.

The comparison between the midline of the fish and the midline of the robot during walking indicated that a single undulation pattern is not sufficient to replicate the motion of the fish. The exact relationship between kinematics and ground interaction is complex; when there is a different amplitude of oscillation between the anterior and of the body, it can change how different sections of the body contact the surface, which influences stability, traction, and directional control. Furthermore, the bioinspired rather than biomimetic nature of the robot resulted in simplifications that affect the interaction between the robot and the ground. Using materials with different frictional coefficients from the fish, constraining motion only in the plane parallel to the surface, and

not producing time-varying gaits all affect the ground reaction forces generated.

Several other directions remain for advancing the capabilities of helix-driven continuum robots. One important direction is the incorporation of soft or compliant elements into the body structure, which could more accurately replicate the flexibility of real fish and enable smoother transitions between curvature states. Another is the development of dynamically adaptable helix geometries, either through variable pitch mechanisms or smart materials, to improve locomotion efficiency by allowing the robot to modulate its gait in response to environmental conditions. Future experiments should also examine the influence of robot-ground interactions on gait stability and propulsion. Finally, integrating proprioceptive sensing or closed-loop control could allow the robot to self-correct for instability and adapt its motion in real time, achieving a level of adaptability closer to that observed in biological organisms.

The robot-twin approach enables a bidirectional pipeline in which biological observations inform robotic design, while robotic experimentation generates new hypotheses about the biomechanics of the animal. By iteratively refining the robot based on fish biological data and analyzing the robot's performance, such as forward velocity, lateral displacement, midline kinematics, and effects of passive appendages we are poised to gain deeper insight into which aspects of the locomotion of *P. senegalus* and other walking fishes are functionally significant for propulsion and stability.

Data availability statement

All data that support the findings of this study are included within the article (and any supplementary files).

Acknowledgments

This work was supported by a Research Grant from the Human Frontier Science Program (HFSP) under Grant ID RGP0010/2022 to VDS and FI. The Grant can be accessed via the following https://doi.org/10.52044/HFSP.RGP00102022.pc.gr.153619.

The biological data was collected at Stockholm University under animal care protocol 11924-2020.

Conflict of interest statement

The authors declare that the research was conducted in the absence of any commercial or financial relationships that could be construed as a potential conflict of interest.

ORCID iDs

Narges Khadem Hosseini 0000-0003-1442-1554
Michael Ishida 0000-0002-6271-3394
Fidji Berio 0000-0003-0810-9783
Valentina Di Santo 0000-0002-5419-3747
Fumiya Iida 0000-0001-9246-7190

References

[1] Pace C and Gibb A C 2014 Sustained periodic terrestrial locomotion in air-breathing fishes *J. Fish Biol.* **84** 639–60
[2] Lauder G V 2022 Robotics as a comparative method in ecology and evolutionary biology *Integr. Comparative Biol.* **62** 721–34
[3] Pfeifer R, Lungarella M and Iida F 2007 Self-organization, embodiment and biologically inspired robotics *Science* **318** 1088–93
[4] Roberts S F, Hirokawa J, Rosenblum H G, Sakhtah H, Gutierrez A A, Porter M E and Long Jr J H 2014 Testing biological hypotheses with embodied robots: adaptations, accidents and by-products in the evolution of vertebrates *Frontiers Robot. AI* **1** 12
[5] Gravish N and Lauder G V 2018 Robotics-inspired biology *J. Exp. Biol.* **221** jeb138438
[6] Standen E M, Du T Y and Larsson H C 2014 Developmental plasticity and the origin of tetrapods *Nature* **513** 54–58
[7] Foster K L, Dhuper M and Standen E M 2018 Fin and body neuromuscular coordination changes during walking and swimming in polypterus senegalus *J. Exp. Biol.* **221** jeb168716
[8] Sfakiotakis M, Lane D M and Davies J B C 1999 Review of fish swimming modes for aquatic locomotion *IEEE J. Ocean. Eng.* **24** 237–52
[9] Blake R W 2004 Fish functional design and swimming performance *J. Fish Biol.* **65** 1193–222
[10] Lauder G V 2015 Fish locomotion: recent advances and new directions *Annu. Rev. Mar. Sci.* **7** 521–45
[11] Marchese A D, Onal C D and Rus D 2014 Autonomous soft robotic fish capable of escape maneuvers using fluidic elastomer actuators *Soft Robot.* **1** 75–87
[12] Zhu J, White C, Wainwright D K, Di Santo V, Lauder G V and Bart-Smith H 2019 Tuna robotics: a high-frequency experimental platform exploring the performance space of swimming fishes *Sci. Robot.* **4** eaax4615
[13] Shintake J, Cacucciolo V, Shea H and Floreano D 2018 Soft biomimetic fish robot made of dielectric elastomer actuators *Soft Robot.* **5** 466–74
[14] Wen L, Wang T, Wu G and Liang J 2012 Quantitative thrust efficiency of a self-propulsive robotic fish: experimental method and hydrodynamic investigation *IEEE/ASME Trans. Mechatronics* **18** 1027–38
[15] Fukui S 1979 On the rock-climbing behavior of the goby, sicyopterus japonicus *Japan. J. Ichthyol.* **26** 84–88
[16] King H M, Shubin N H, Coates M I and Hale M E 2011 Behavioral evidence for the evolution of walking and bounding before terrestriality in sarcopterygian fishes *Proc. Natl Acad. Sci. 1* **108** 21146–51
[17] Bressman N R, Morrison C H and Ashley-Ross M A 2021 Reffling: a novel locomotor behavior used by neotropical armored catfishes (loricariidae) in terrestrial environments *Ichthyol. Herpetol.* **109** 608–25
[18] Lucifora L O and Vassallo A I 2002 Walking in skates (chondrichthyes, rajidae): anatomy, behaviour and analogies to tetrapod locomotion *Biol. J. Linnean Soc.* **77** 35–41
[19] Pace C and Gibb A 2009 Mudskipper pectoral fin kinematics in aquatic and terrestrial environments *J. Exp. Biol.* **212** 2279–86
[20] McInroe B, Astley H C, Gong C, Kawano S M, Schiebel P E, Rieser J M, Choset H, Blob R W and Goldman D I 2016 Tail

use improves performance on soft substrates in models of early vertebrate land locomotors *Science* **353** 154–58
[21] Ning L, Limpabandhu C and Tse Z T H 2024 Amphibian-inspired locomotion strategy for a slime-based magnetic soft robot *Robot. Rep.* **2** 152–65
[22] Lin Z, Zheng W, Zhang J, Ou W, Yang C, Huang H, Xu W, Yang Z, Zhou W and Zhang Y 2023 Mudskipper-inspired amphibious robotic fish enhances locomotion performance by pectoral-caudal fins coordination *Cell Rep. Phys. Sci.* **4** 101589
[23] Hirose S 1993 *Biologically Inspired Robots: Serpentile Locomotors and Manipulators* (Oxford University Press, Inc)
[24] Wright C, Johnson A, Peck A, McCord Z, Naaktgeboren A, Gianfortoni P, Gonzalez-Rivero M, Hatton R and Choset H 2007 Design of a modular snake robot *2007 IEEE/RSJ Int. Conf. on Intelligent Robots and Systems* (IEEE) pp 2609–14
[25] Ijspeert A J 2020 Amphibious and sprawling locomotion: from biology to robotics and back *Ann. Rev. Control Robot. Auton. Syst.* **3** 173–93
[26] Suzuki S, Kano T, Ijspeert A J and Ishiguro A 2021 Spontaneous gait transitions of sprawling quadruped locomotion by sensory-driven body–limb coordination mechanisms *Front. Neuroroboti.* **15** 645731
[27] Seok S, Onal C D, Cho K J, Wood R J, Rus D and Kim S 2012 Meshworm: a peristaltic soft robot with antagonistic nickel titanium coil actuators *IEEE/ASME Trans. Mechatronics* **18** 1485–97
[28] Daltorio K A, Boxerbaum A S, Horchler A D, Shaw K M, Chiel H J and Quinn R D 2013 Efficient worm-like locomotion: slip and control of soft-bodied peristaltic robots *Bioinsp. Biomim.* **8** 035003
[29] Karakasiliotis K, Thandiackal R, Melo K, Horvat T, Mahabadi N K, Tsitkov S, Cabelguen J-M and Ijspeert A J 2016 From cineradiography to biorobots: an approach for designing robots to emulate and study animal locomotion *J. R. Soc. Interface* **13** 20151089
[30] Brainerd E L, Baier D B, Gatesy S M, Hedrick T L, Metzger K A, Gilbert S L and Crisco J J 2010 X-ray reconstruction of moving morphology (xromm): precision, accuracy and applications in comparative biomechanics research *J. Exp. Zool. A* **313** 262–79
[31] Akanyeti O, Di Santo V, Goerig E, Wainwright D K, Liao J C, Castro-Santos T and Lauder G V 2022 Fish-inspired segment models for undulatory steady swimming *Bioinsp. Biomim.* **17** 046007
[32] Webb B 2001 Can robots make good models of biological behaviour? *Behav. Brain Sci.* **24** 1033–50
[33] Ishida M, Berio F, Di Santo V, Shubin N H and Iida F 2024 Paleoinspired robotics as an experimental approach to the history of life *Sci. Robot.* **9** eadn1125
[34] Full R J and Koditschek D E 1999 Templates and anchors: neuromechanical hypotheses of legged locomotion on land *J. Exp. Biol.* **202** 3325–32
[35] Raibert M H 1986 *Legged Robots That Balance* (MIT press)
[36] Floyd S and Sitti M 2008 Design and development of the lifting and propulsion mechanism for a biologically inspired water runner robot *IEEE Transact. Robot.* **24** 698–709
[37] Zhong Y, Li Z and Du R 2017 A novel robot fish with wire-driven active body and compliant tail *IEEE/ASME Trans. Mechatronics* **22** 1633–43
[38] Lin H T and Trimmer B A 2010 The substrate as a skeleton: ground reaction forces from a soft-bodied legged animal *J. Exp. Biol.* **213** 1133–42
[39] Suzuki S, Fukuhara A, Owaki D, Kano T, Ijspeert A J and Ishiguro A 2017 A simple body-limb coordination model that mimics primitive tetrapod walking *2017 56th Annual Conf. Society of Instrument and Control Engineers of Japan (SICE)* pp 12–14
[40] Gevers L, Gupta A, Paez L, Fu Q, Standen E and Ijspeert A 2025 Investigating the effect of morphology on the terrestrial gaits of amphibious fish using a reconfigurable robot *Bioinspir. Biomim.* **20** 046002
[41] Zarrouk D, Mann M, Degani N, Yehuda T, Jarbi N and Hess A 2016 Single actuator wave-like robot (saw): design, modeling and experiments *Bioinsp. Biomim.* **11** 046004
[42] Liu S *et al* 2023 Grounding dino: marrying dino with grounded pre-training for open-set object detection (arXiv:2303.05499)
[43] Kirillov A *et al* 2023 Segment anything *Proc. IEEE/CVF Inter. Conf. on Computer Vision* pp 4015–26
[44] Saha P K, Borgefors G and di Baja G S 2017 Skeletonization and its applications–a review *Skeletonization: Theory, Methods and Applications* (Academic) pp 3–42
[45] van der Walt S, Schönberger J L, Nunez-Iglesias J, Boulogne F, Warner J D, Yager N, Gouillart E and Yu T 2014 scikit-image: image processing in python *PeerJ* **2** e453
[46] Hainer J C, Lutek K, Maki H and Standen E M 2023 Sensorimotor control of swimming polypterus senegalus is preserved during sensory deprivation conditions across altered environments *J. Exp. Biol.* **226** jeb245192
[47] Jocher G and Qiu J 2024 Ultralytics yolo11 (available at: https://github.com/ultralytics/ultralytics)